AS-TEXONO/03-05
June 21, 2003

Near Threshold Pulse Shape Discrimination Techniques in Scintillating CsI(Tl) Crystals

S.C. Wu[a,b], Q. Yue[c,d], W.P. Lai[a,e], H.B. Li[a,b], J. Li[c,d], Y. Liu[c], M.Z. Wang[b], H.T. Wong[a,*], B. Xin[f], Z.Y. Zhou[f]

[a]Institute of Physics, Academia Sinica, Taipei 115, Taiwan.
[b]Department of Physics, National Taiwan University, Taipei 106, Taiwan.
[c]Institute of High Energy Physics, Beijing 100039, China.
[d]Department of Engineering Physics, Tsing Hua University, Beijing 100084, China
[e]Department of Management Information Systems, Chung Kuo Institute of Technology, Hsin-Chu 303, Taiwan.
[f]Department of Nuclear Physics, Institute of Atomic Energy, Beijing 102413, China

Abstract

There are recent interests with CsI(Tl) scintillating crystals for Dark Matter experiments. One of the major experimental challenges is to differentiate nuclear recoil signatures from the background β/γ-events due to ambient radioactivity on the basis of their different pulse shapes in the domain where the light output is close to the detection threshold. Using data derived from measurements with low energy γ's and nuclear recoils due to neutron elastic scatterings, several methods of pulse shape discrimination are studied, and their relative merits are compared. Full digitization of the pulse shapes is crucial to achieve good discrimination. Advanced software techniques with mean time, neural network and likelihood ratios give rise to satisfactory performance, and are superior to the conventional Double Charge method commonly applied at higher energies. Pulse shape discrimination becomes effective at a light yield of at least 10 photo-electrons. This corresponds to a detection threshold of 2−3 keV electron-equivalence energy, or 15−20 keV recoil kinetic energy, in realistic experiments.

PACS Codes: 29.40.Mc, 07.05.Kf, 84.35.+i.
Keywords: Scintillation detectors, Data analysis, Neural Networks.

(Submitted to Nucl. Instrum. Methods A)

*Corresponding author: Email: htwong@phys.sinica.edu.tw; Tel:+886-2-2789-6789; FAX:+886-2-2788-9828.

1 Introduction

The detection of Dark Matter and the studies of their properties [1] are of fundamental importance in particle physics and cosmology. The Weakly Interacting Massive Particles (WIMPs) are good candidates for "Cold Dark Matter", and their experimental searches have gathered a lot of interests in recent years. The most promising avenue is to detect the nuclear recoil signatures due to elastic scatterings of WIMPs on the target isotopes. The typical energy depositions are only of the order of 10 keV, imposing big experimental challenges in terms of the detection of weak signals as well as background control at low energy close to detection threshold. A wide spectrum of experimental techniques is being pursued [1]. There is still much room for new detector concept to push the sensitivities further. It would be of great interest if the sensitivities of WIMP searches can probe the level predicted by the various Super-Symmetry models.

There are potential merits of using CsI(Tl) scintillating crystals [2] for WIMP search and other low-energy low-background experiments [3, 4]. An experiment with 200 kg of CsI(Tl) crystal scintillators to study low energy neutrino interactions at the Kuo-Sheng power reactor is being pursued [4, 5], while the adaptation of the crystal for Dark Matter searches are the focus of several on-going projects [6, 7, 8, 9].

The high-A content of the CsI enhances the sensitivities for the spin-independent interactions (which depends on the neutron number squared) between the WIMPs and the target, relative to most other candidate target isotopes. The high-Z composition allows a compact design and provides large suppression of background due to ambient radioactivity if a three dimensional fiducial volume definition can be realized. Both ^{133}Cs and ^{127}I are 100% in their respective isotopic abundance. Being close in their mass numbers, the response to nuclear recoil from the interactions with WIMPs would be similar, allowing simpler interpretations of the experimental signatures.

As a detector, the crystal has large light yield, low energy threshold and with pulse shape discrimination (PSD) characteristics for differentiating β/γ background from the nuclear recoil events [2, 5]. Scintillating NaI(Tl) crystals with the order of 100 kg target mass have been deployed for Dark Matter experiments [10], but it has been shown that CsI(Tl) provides superior PSD capabilities to NaI(Tl) [6]. Unlike NaI(Tl), CsI(Tl) is only slightly hygroscopic such that it can be machined easily and does not require hermetic seal (that is, passive materials) in a large detector system. In addition, large (40 tons) electromagnetic calorimeter systems [11] have been constructed and made operational in high energy physics experiments, making this technology affordable and realistic to scale up. Considering all the associated costs, the price of CsI(Tl) is in fact less than that for NaI(Tl). In order to produce positive and definite evidence of the WIMPs, an accurate

measurement of the annual modulation (where the maximal effects are only 7%) would be necessary such that the availability of large target mass is a very desirable feature.

One of the key issues to realize a Dark Matter search experiment with CsI(Tl) crystal scintillator is the studies of the experimental signatures of nuclear recoils due to WIMP-nuclei elastic scatterings. Nuclear recoils produce high charge density (dE/dx) such that the scintillating light yield is "quenched" and the timing profile of pulse shape is different relative to the same energy deposition by minimum ionizing particles [12]. These WIMP-induced signatures are the same as the nuclear recoil events produced by elastic scattering of neutrons on nuclei, and hence can be studied in the laboratory.

This article reports on the studies of pulse shape discrimination to differentiate nuclear recoil events from β/γ background in CsI(Tl) crystal scintillator in the light yield regime close to the detection threshold.

2 Pulse Shape Discrimination

2.1 Basics

The light emission profiles of scintillating CsI(Tl) crystals exhibit different shape for γ-rays and electrons (that is, minimum ionizing particles), as compared to that for α-particles and nuclear recoils, as depicted in the Flash Analog Digital Convertor (FADC) measurements in Figure 1. Heavily ionizing events due to α-particles and nuclear recoils have *faster* decays than those from e/γ's – opposite to the response in liquid scintillator [12]. This characteristic property makes particle identification possible with this scintillator [13].

Fitted the pulse shape(A) as a function of time(t) to an analytical form of

$$\mathrm{A} = \mathrm{Constant} * [\ 1 - \exp(-\frac{\mathrm{t}}{\tau_0})\ ] * [\ \frac{1}{\tau_1}\ \exp(-\frac{\mathrm{t}}{\tau_1}) + \frac{\mathrm{r}}{\tau_2}\ \exp(-\frac{\mathrm{t}}{\tau_2})\ ] \qquad (1)$$

for the light profiles of γ/α events, one obtains the fitted-values of rise time(τ_0) and fall times(τ_1, τ_2) as well as the ratio between the slow and fast decay components(r) as tabulated in Table 1. For comparison, those for undoped CsI crystal are also shown. The values of τ_0 in CsI(Tl) are dominated by the electronics shaping rise time of 250 ns for $> \mu$s pulses [14]. The intrinsic rise times of the CsI(Tl) scintillator are expected to $\sim$125 ns and $\sim$20 ns for γ- and α-events, respectively [2].

The difference in the decay time constants between the γ's and the nuclear recoils forms the basis of PSD. Matured PSD techniques have been devised at high energies where the photo-electrons are abundant. The experimental challenge for adapting the

PSD idea to Dark Matter experiments is that one must now work in the regime where the number of photo-electrons (N_{pe}) is small. In the following sub-sections, we investigate and compare the performance in PSD at this low light output domain with different software techniques.

2.2 Measurements and Data Samples

A CsI(Tl) crystal of dimensions 5 cm $\times$ 5 cm $\times$ 5 cm was used to provide data for these investigations. The light emissions were read out by a 29 mm diameter photo-multiplier tube (PMT)[†] with standard bi-alkali photo-cathode. The conversion factor between energy deposition and light output is 4 photo-electron per keV of electron-equivalence energy. This was obtained by calibration measurements with an LED pulser operated at the $N_{pe} \sim 1$ intensity. The events were digitized by a 20 MHz (that is, 50 ns for one time-bin) FADC [14] with 8-bit resolution, such that the pulse shape can be denoted by an amplitude time-sequence A_i.

Data were taken with standard radioactive γ (^{55}Fe: 5.9 keV; ^{109}Cd: 22.1 keV ; ^{137}Cs: 662 keV) and α (^{241}Am: 5.49 MeV) sources. Nuclear recoil data, on the other hand, were taken from the neutron facility at the 13 MV Tandem accelerator at the China Institute of Atomic Energy at Beijing. The data consisted of Time-of-Flight (ToF) measurements which helped to distinguish nuclear recoil from the other background events. The results of the quenching factor measurements were already published [9].

The nuclear recoil pulses recorded in a neutron beam environment were contaminated by an intense accidental γ-background. The average pulse shapes for both nuclear recoil and γ-background (as identified by the ToF cut) events derived from the neutron beam measurements are depicted in Figure 2. Upon taking averages from a large sample and subtracting an offset, such data are sufficient to provide a good quenching factor measurement as well as the average *"background-free"* nuclear recoil pulse shape displayed in Figure 1. The energy dependence of the nuclear recoil profile is small compared to the differences in the pulse shapes between the recoil and γ-events shown in Figure 1.

However, at the event-by-event level, the time-profile for photo-electron emissions is complicated by an uncontrolled and sizable background contribution. Dark Matter searches, on the other hand, are low-count-rate experiments such that nuclear recoils due to WIMP interactions will *not* be contaminated by accidentals. Therefore the neutron beam data do not provide a realistic sample for the studies of detector response in WIMP searches at the event-by-event level.

[†]CR110, Hamamatsu Photonics, China

As remedies, the single-event nuclear recoil pulse shape was generated by simulations, using as input the measured pulse profiles of Figure 1 and the parametrization of Table 1. The LED pulser measurements provided the single photo-electron response of the PMT and readout system. The simulated events were convolutions of several of these single photo-electron pulses whose timing is distributed according to the average recoil pulse shape. A "self-trigger" criterion was imposed to mimic the realistic situation – that is, the time-zero of the events was defined by the first instants where the pulse was above a specified threshold. As illustrations, typical events at $N_{pe} \sim 20$ from the measured γ and simulated nuclear recoil data are displayed in Figure 3a and 3b, respectively. Both categories of events are similar by visual inspection, demonstrating that (a) the simulation algorithms are valid, and (b) advanced pattern recognition techniques would be necessary to achieve event identification.

Using the same algorithm but a different reference profile, simulated γ-events were also generated. The data samples with simulated nuclear recoil and γ events, denoted by D_{nr} and D_{γ}, respectively, were adopted in the PSD studies discussed below. The choice of simulated events instead of measurements with low energy sources (^{55}Fe, ^{109}Cd) for the γ samples allows a continuous scan of the input light yield in units of N_{pe}. Residual systematic effects are also minimized and canceled out when comparisons are made among simulated samples. Applying the various PSD methods to the measured γ data would produce consistent results.

2.3 Classical Pulse Shape Discrimination Method

2.3.1 Double Charge Method

A well-established way to achieve PSD at high light yield is the "double charge method" [15]. This involves the comparison of the "total charge" (Q_t) and the "partial charge" (Q_p), which are the total and partial integration of the pulse, respectively. This is the standard approach with Analog Digital Convertor (ADC) based data acquisition systems where the complete pulse shape information is not available. Typically, the partial charge measurement is done by delaying the PMT pulses via cabling and both the prompt and delayed signals are read out by the ABC sampled with the same gate.

Displayed in Figure 4 is the comparison of γ and α events at the MeV energy range from data with ambient radioactivity and ^{241}Am α-source, respectively. The ranges were chosen such that Q_t and Q_p involve integration over 4 μs after trigger and *after* a delay of 0.5 μs, respectively. A γ/α separation of >99% efficiency down to about 200 keV electron-equivalence light output can be achieved. It has been shown that PSD can be

achieved even in high energy events where the FADC measurements are saturated [16]. However, as indicated in Figure 4, one would come into difficulties to perform PSD with this simple algorithm for events at light yield below 100 keV electron-equivalence energy.

2.4 Pulse Shape Discrimination Methods at Full Digitization

With the advent and popular usage of FADCs, complete pulse shape digitization becomes realistic. Three different pattern recognition techniques were investigated, all of which rely on the full digitization of the PMT signals.

2.4.1 Mean Time Method

The measurement of the average time for individual events by the mean time (MT) method has been used for PSD studies [6]. The mean time is defined as

$$\langle t \rangle \;=\; \frac{\sum\limits_{i}\;(A_i\;t_i)}{\sum\limits_{i}\;A_i} \quad , \tag{2}$$

where A_i is the FADC-amplitude at time-bin t_i.

The typical $\langle t \rangle$ distributions at $N_{pe} \sim 20$ for D_{nr} and D_γ are displayed in Figure 5a, at an integration of 2.5 μs after the time-zero set by the trigger. It can be seen that satisfactory separation can be achieved under such conditions.

2.4.2 Neural Network Methods

The neural network (NN) methods [17] are now frequently adopted for analysis in high energy physics experiments. It has been applied to event-by-event pulse shape analysis for background identification in double beta decay searches [18]. The pedestal-subtracted FADC data within 2.5 μs after trigger corresponds to the input nodes of the neural network. That is, the network has N_i=50 input nodes denoted by $X(x_i)$ with the integrated sum normalized to unity:

$$\sum_{i=1}^{N_i} x_i = 1 \; . \tag{3}$$

Negative values were reset to zero. In addition, there were N_h=25 hidden nodes.

Adopting the Neural Network JETNET 3.0 package [17], a function F(X) is defined such that

$$F(X) \;=\; G(\sum_{j=1}^{N_h} u_j \; G(\sum_{k=1}^{N_i} w_{jk} \; x_k + \theta_j) + \phi_0) \tag{4}$$

where (u_j, w_{jk}) and (θ_j, ϕ_0) are the "weight" and "offset" coefficients, respectively, to be derived from the training samples, and the function G(y) is the non-linear neuron activation function

$$G(y) \;=\; \frac{1}{2}\,[\,1+\tanh(y)\,] \;=\; \frac{1}{1+e^{-2y}} \qquad , \tag{5}$$

which is the functional form characterizing a 3-layer neural network consisting of the input, hidden and output layers.

A total of N_t=4000 events from both the D_{nr} and D_γ data sets are used as training samples, corresponding to T(X)=1 and 0, respectively. The optimal coefficients are obtained by minimizing the error function

$$E \;=\; \sum_{i=1}^{N_t} \,[\,F(X)-T(X)\,]^2 \quad . \tag{6}$$

Once the coefficients are derived, the procedures are applied to *independent* data set from D_{nr} and D_γ. The typical F(X) distributions at $N_{pe} \sim 20$ are displayed in Figure 5b, showing good separation among them.

2.4.3 Likelihood Ratio Methods

Motivated by the commonly-used of likelihood ratio test [1, 19] for the goodness-of-fit, a likelihood ratio (LR) method was devised to perform the tasks of pulse shape analysis. Similar methods are successfully applied in high energy physics data analysis in comparing likelihoods and assigning probabilities among the different hypotheses for events where many output parameters are measured. The reference profiles for neutrons and γ's from Figure 1 are required as the input. This is different from the previous two techniques where prior knowledge of the reference profiles is not necessary.

The areas of the reference pulses are normalized to unity, and the profiles are denoted by arrays $R(r_i)$ and $\Gamma(\gamma_i)$ for the nuclear recoil and γ reference shapes, respectively. Two likelihood functions, L_r and L_γ, are defined for each event:

$$L_r \;=\; \prod_{i=1}^{N_i} r_i^{x_i} \quad ; \quad L_\gamma \;=\; \prod_{i=1}^{N_i} \gamma_i^{x_i} \quad , \tag{7}$$

where $X(x_i)$ with dimension $N_i = 50$ are the measured pulse shape information for the events to be analyzed, as defined in Section 2.4.2. The likelihood functions quantify how probable the measured pulse shapes do originate from the the reference profiles. The likelihood ratio LR defined by:

$$LR \;=\; \frac{L_r}{L_r + L_\gamma} \quad , \tag{8}$$

will test which hypothesis is more likely such that LR will be larger and less than 0.5 for nuclear recoil and γ events, respectively.

The algorithm is applied to the D_{nr} and D_γ data set. The typical LR distributions at $N_{pe} \sim 20$ are depicted in Figure 5c. The separation between the two data samples is satisfactory.

2.5 Comparisons

To compare the performance of the three methods on D_γ and D_{nr}, two figures of merits are defined: (a) ϵ_{90}: the survival efficiencies of D_{nr} at selections which ensure that 90% of the D_γ events are suppressed; and (b) λ_{90}: the probabilities where the D_γ events would be mis-identified as recoil signals at cuts where 90% of D_{nr} would survive. Both ϵ_{90} and λ_{90} are energy dependent, and would approach 1 and 0, respectively, at the high light yield (large N_{pe}) limits.

The variations of ϵ_{90} and λ_{90} as a function of N_{pe} for the three different methods (MT, NN, LR) are depicted in Figures 6a and 6b, respectively. The photo-electron number N_{pe} was adopted as the unit to characterize the light yield. In this way, the results can be directly applicable to other configurations using CsI(Tl) as the detector medium. Dotted lines in Figures 6a and 6b corresponds to the survival probabilities of D_γ and D_{nr}, respectively. The results indicate that all the three methods: (a) can achieve PSD with satisfactory efficiencies (>40% γ-background rejection) at $N_{pe} > 10$; (b) can identify >90% of the D_γ background while keeping the efficiencies for D_{nr} to be >90% at $N_{pe} > 60$; and (c) give similar performance among themselves, although the spread of the data points as functions of N_{pe} suggests that the LR method may subject to larger systematic uncertainties, or alternatively, the LR method is more sensitive to the tunings in the software parameters.

Tests have been performed on simulated events with different single photo-electron response functions. It is found that the performance parameters shown in Figures 6a and 6b remain unchanged. This shows that the results are robust and insensitive to the details of the simulation algorithms so long as the reference profiles in Figure 1 are used for the photo-electron timing distributions. Alternatively, this indicates that the PSD methods are also valid in measurements of CsI(Tl) crystals with different PMT response and electronics settings like the shaping times.

3 Summary and Conclusions

This article reports on the studies on the applications of various software techniques to achieve pulse shape discrimination near detector threshold for CsI(Tl) crystal scintillator. The performance of the three methods based on complete pulse shape information (mean time, neural network and likelihood ratio) is superior to the matured and conventional double charge method well-demonstrated when photo-electrons are abundant. Full digitization is crucial for achieving PSD at the marginal statistics domain. There is no big difference in the performance among the three PSD methods. The algorithms are robust and insensitive to the measurement parameters like PMT response or electronic shaping times.

The results from this study are relevant to the potential capabilities and practical design of Dark Matter experiments based on the CsI(Tl) crystal. Satisfactory separation between γ and nuclear recoil events can be achieved when the photo-electron statistics is larger than 10, which corresponds to an electron-equivalence energy threshold of $2-3$ keV, or $15-20$ keV recoil kinetic energy, in the adopted detector configuration of 0.56 kg target mass. In realistic Dark Matter experiments, the modular mass for the CsI(Tl) target will have to be bigger, such as at the range of several kg. To maintain or even improve on such threshold, the light transmission within the crystal and from the crystal to the PMT photo-cathode will have to be optimized. Larger PMT readout surfaces as well as green-extended photo-cathodes to match the spectral emissions of CsI(Tl) can be used.

Although the studies focus on data with CsI(Tl) crystal scintillators for Dark Matter searches, the techniques can be readily applied to other detector systems for other experiments where the pulse shapes of individual events can provide information of their identification. The conclusions on the relative merits among the different PSD methods are expected to be applicable to other pulse shape analysis problems where the statistics are marginal.

Besides differentiating β/γ-background from nuclear recoil events, these studies may help to lower the detection threshold by suppressing electronic noise and microphonism where the pulse shapes are in general different from those of the signals. Experiments which need *both* low threshold and background may potentially benefit from these techniques. Alongside with Dark Matter experiments, such requirements are critical in the search of neutrino magnetic moments [4] and in the measurement of the coherent scatterings of the neutrinos on the nuclei [20].

The authors would like to thank Drs. S.K. Kim and Y.D. Kim for fruitful discussions and helpful comments, and are grateful to the technical staff from CIAE and IHEP for the

neutron beam data. This work was supported by contracts CosPa 89-N-FA01-1-4-2 from the Ministry of Education, Taiwan, NSC 89-2112-M-001-056, NSC 90-2112-M-001-037 and NSC 91-2112-M-001-036 from the National Science Council, Taiwan, and NSF19975050 from the National Science Foundation, China.

References

[1] See the respective sections in *Review of Particle Physics*, Particle Data Group, Phys. Rev. **D 66** (2002), for details and references.

[2] H. Grassmann, E. Lorentz and H.G. Moser, Nucl. Instrum. Methods **228**, 323 (1985); P. Schotanus, R. Kamermans, and P. Dorenbos, IEEE Trans. Nucl. Sci. **37**, 177 (1990).

[3] H.T. Wong et al., Astropart. Phys. **14**, 141 (2000).

[4] H.T. Wong and J. Li, Mod. Phys. Lett. **A 15**, 2011 (2000);
H.B. Li et al., TEXONO Coll., Nucl. Instrum. Methods **A 459**, 93 (2001);
H.B. Li et al., TEXONO Coll., Phys. Rev. Lett. **90**, 131802 (2003).

[5] Y. Liu et al., TEXONO Coll., Nucl. Instrum. Methods **A 482**, 125 (2002).

[6] G. Gerbier et al., Astropart. Phys. **11**, 287 (1999);
S. Pecourt et al., Astropart. Phys. **11**, 457 (1999).

[7] V.A. Kudryavtsev et al., Nucl. Instrum. Methods **A 456**, 272 (2001).

[8] H.J. Kim et al., Nucl. Instrum. Methods **A 457**, 471 (2001).

[9] M.Z. Wang et al., Phys. Lett. **B 536**, 203 (2002).

[10] R. Bernabei et al., Phys. Lett.**B 480**, 23 (2000), and references therein.

[11] Y. Kubota et al., CLEO Coll., Nucl. Instrum. Methods **A 320**, 66 (1992);
E. Aker et al., Crystal Barrel Coll., Nucl. Instrum. Methods **A 321**, 69 (1992);
K. Miyabayashi, Belle Coll., Nucl. Instrum. Methods **A 494**, 298 (2002);
B. Lewandowski, BaBar Coll., Nucl. Instrum. Methods **A 494**, 303 (2002).

[12] See, for example, J.B. Birks, *Theory and Practice of Scintillation Counting*, Pergamon (1964).

[13] J. Alarja et al., Nucl. Instrum. Methods **A 242**, 352 (1982);
F. Benrachi et al., Nucl. Instrum. Methods **A 281**, 137 (1989).

[14] W.P. Lai et al., TEXONO Coll., Nucl. Instrum. Methods **A 465**, 550 (2002).

[15] C.L. Morris et. al., Nucl. Instrum. Methods **137**, 397 (1976);
M.S. Zucker and N. Tsoupas, Nucl. Instrum. Methods **A 299**, 281 (1990).

[16] Q. Yue, hep-ex/0304022, in press, Nucl. Instrum. Methods **A** (2003).

[17] See, for example,
C. Peterson, T. Rognvaldsson and L. Lonnblad, Comput. Phys. Comm. **81**, 185 (1994);
C.M. Bishop, *Neural Networks for Pattern Recognition*, Clarendon Press, Oxford (1995).

[18] B. Majorovitis and H.V. Klapdor-Kleingrothaus, Eur. Phys. J. **A 6**, 463 (1999).

[19] S. Baker and R.D. Cousins, Nucl. Instrum. Methods **221**, 125 (1984), and references therein.

[20] H.B. Li and H.T. Wong, J. Phys. **G 28**, 1453 (2002).

Crystal	Event Type	Rise Time	Decay Time Constant		Ratio (r)
		$[\tau_0$ (ns)]	Fast Comp. $[\tau_1$ (μs)]	Slow Comp. $[\tau_2$ (μs)]	
CsI(Tl)	α	203±3	0.54±0.1	2.02±0.02	0.29±0.02
CsI(Tl)	γ	261±2	0.87±0.1	5.20±0.04	0.61±0.01
CsI(pure)	γ	∼0.55	0.19±0.01	–	–

Table 1: Fitted rise and decay time constants as well as the ratio between slow and fast decay components for α and γ events measured by CsI(Tl) and undoped CsI.

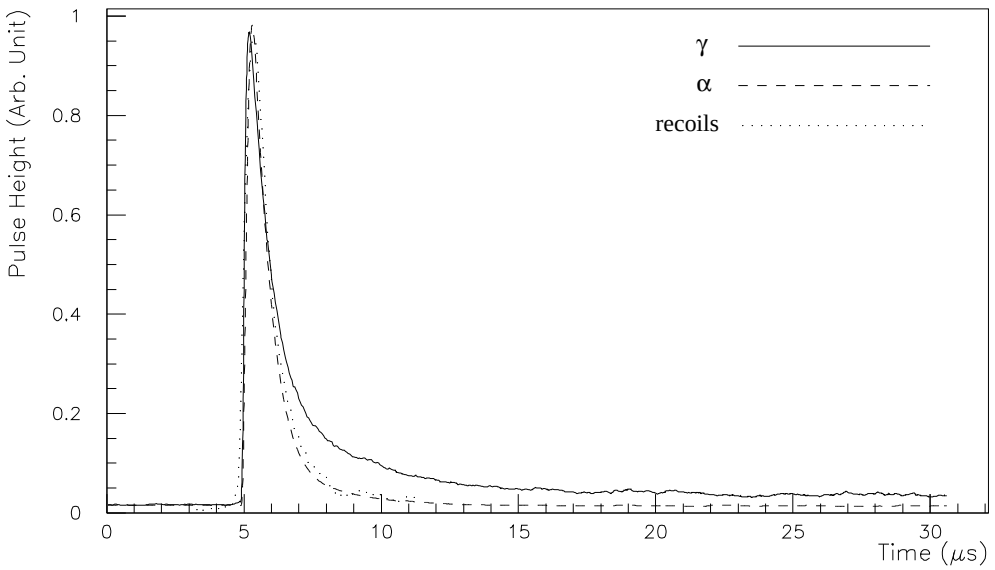

Figure 1: The average pulse shapes of events due to γ-rays and α-particles from direct measurements and background-free nuclear recoils derived from the neutron beam data.

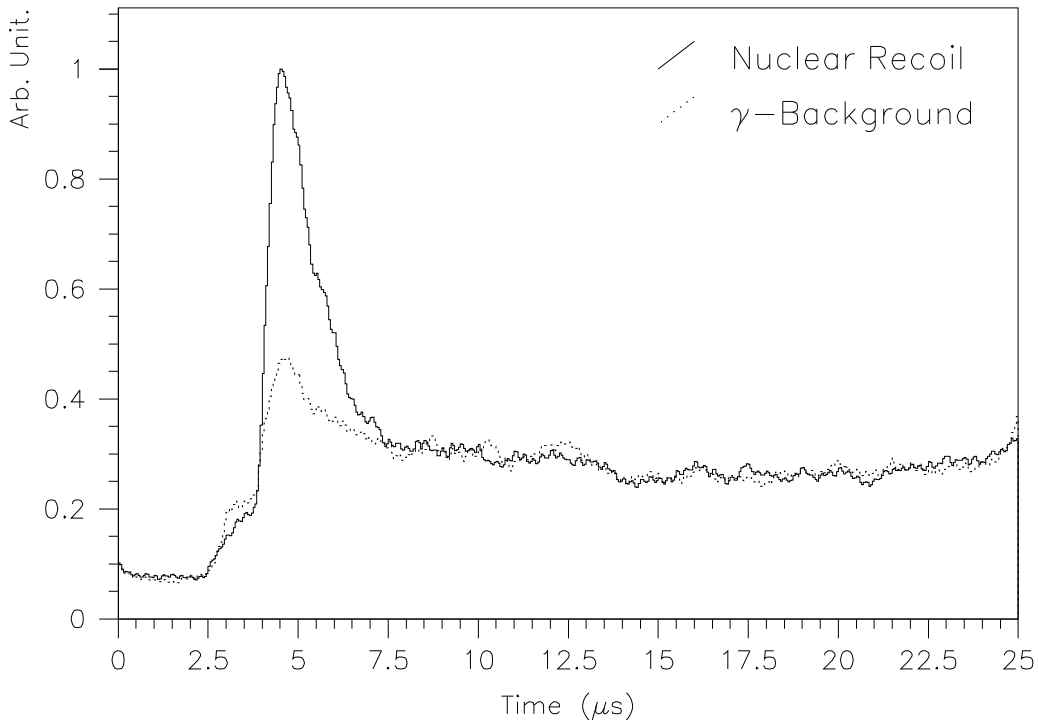

Figure 2: The average pulse shapes for the nuclear recoil and γ-background events directly from the neutron beam measurements.

(a)

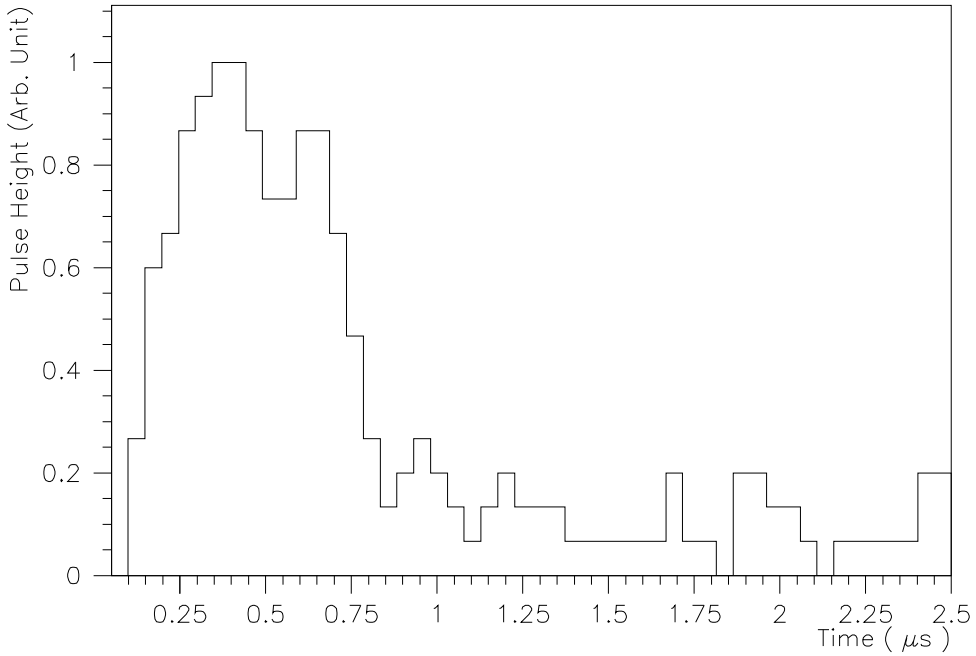

(b)

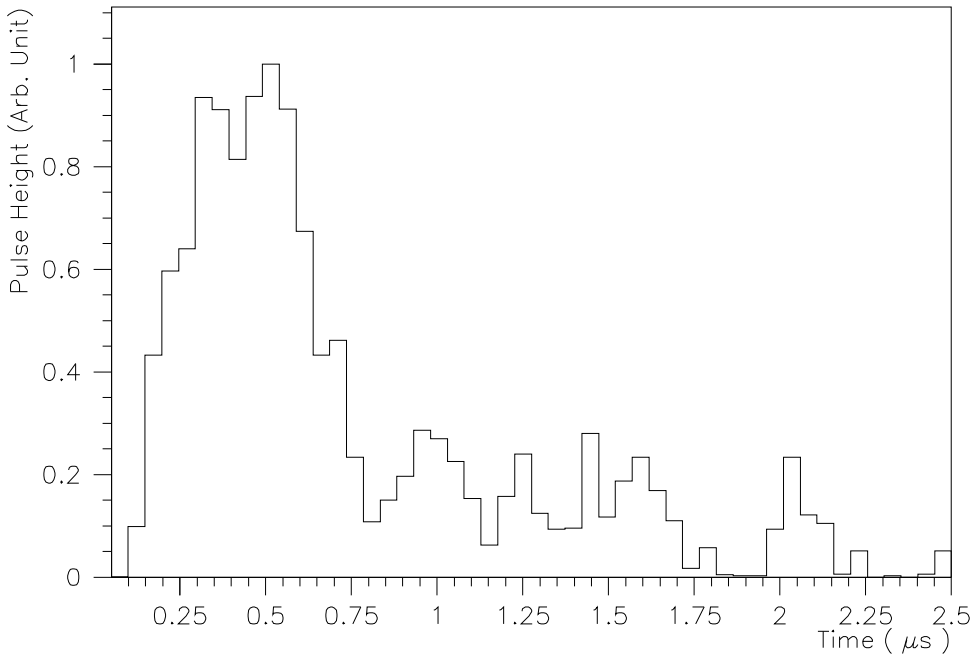

Figure 3: Typical single (a) measured γ- and (b) simulated nuclear recoil events at $N_{pe} \sim 20$.

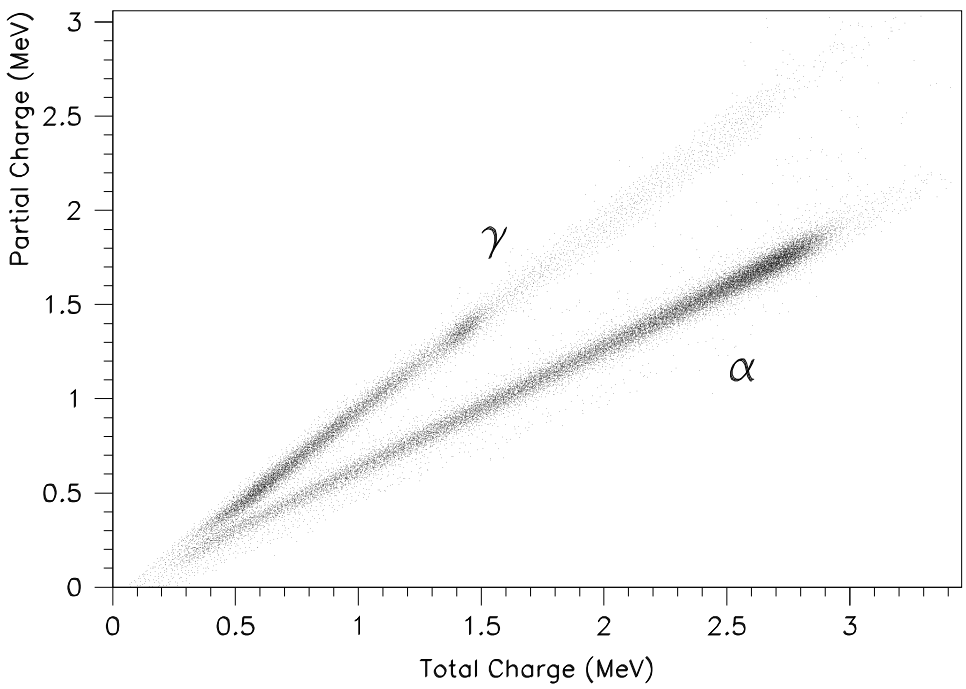

Figure 4: The partial charge versus total charge at the high (MeV) energy range in a CsI(Tl) crystal, showing excellent (>99%) pulse shape discrimination capabilities to differentiate events due to α's and γ's. The α-events are from an ^{241}Am source placed on the surface of the crystal, while the γ-events are due to ambient radioactivity.

(a)

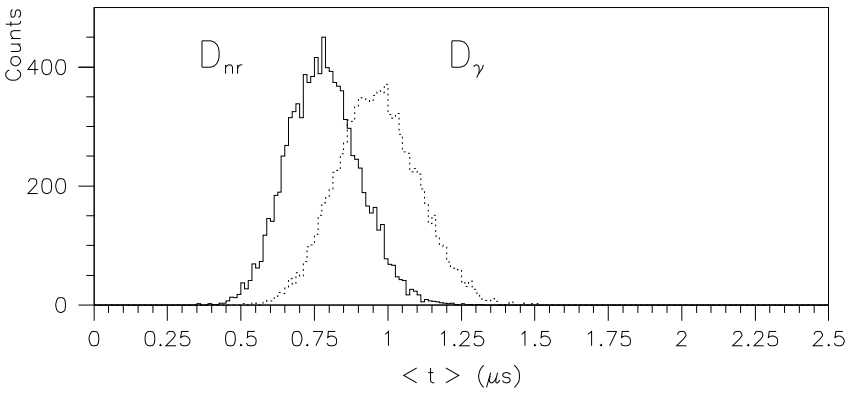

(b)

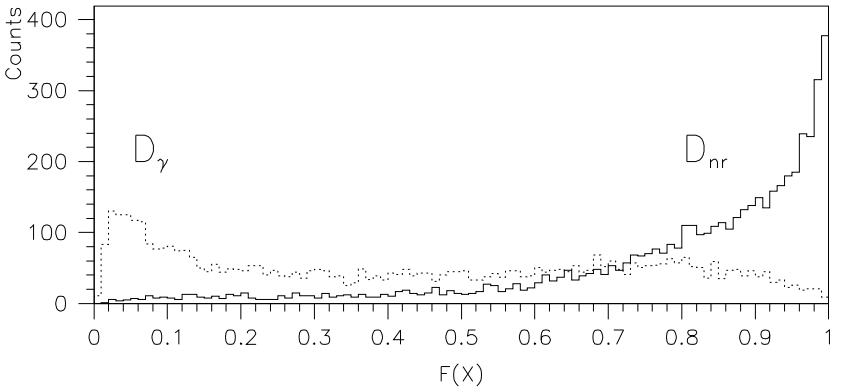

(c)

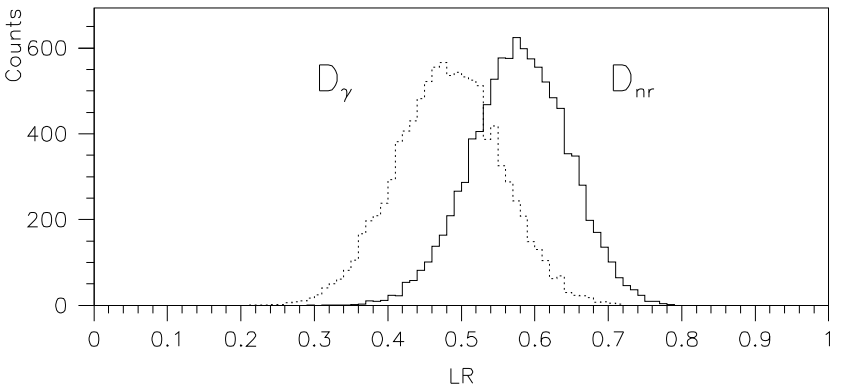

Figure 5: Typical separations of the (a) $\langle t \rangle$, (b) F(X) , and (c) LR parameters at $N_{pe} = 20$ between nuclear recoil (D_{nr}, in solid histograms) and γ (D_γ, in dotted histograms) events with the mean time, neural network and likelihood ratio methods, respectively.

(a)

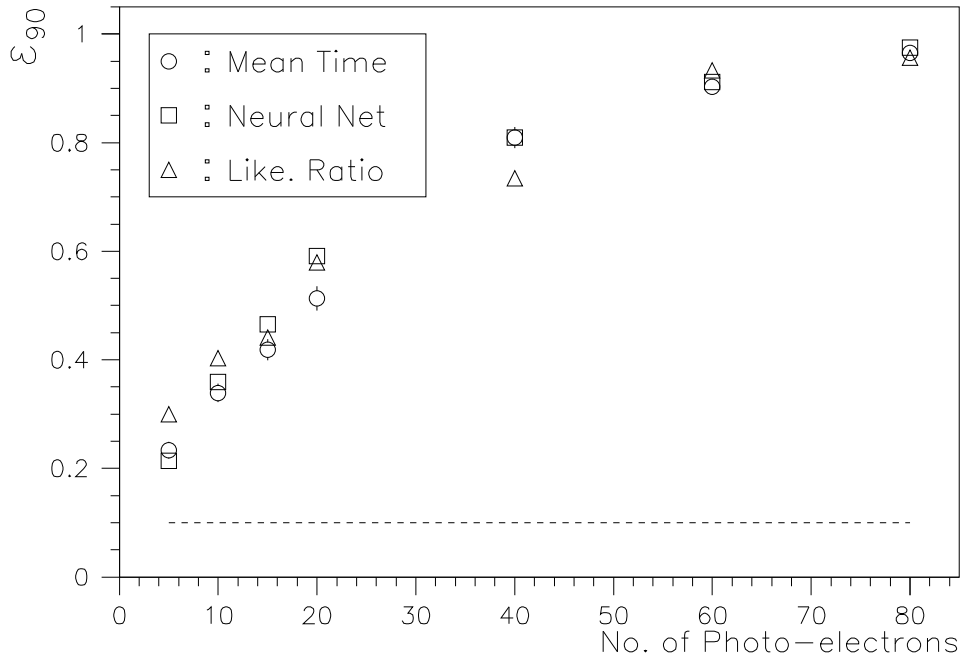

(b)

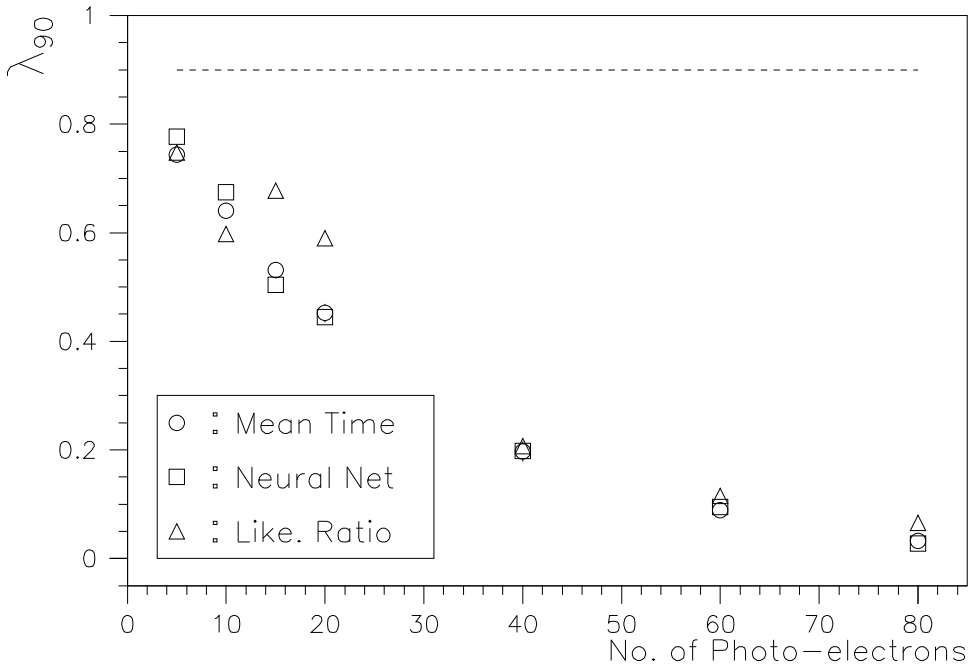

Figure 6: The variations of the figures of merit (a) ϵ_{90} and (b) λ_{90} with N_{pe} with the three different techniques applied to simulated nuclear recoil and γ data, respectively. Dotted lines indicate survival probabilities of γ and recoil events in (a) and (b), respectively. The statistical uncertainties are smaller than the data points.